ELSEVIER

Journal of Organometallic Chemistry 632 (2001) 49–57

Journal of Organometallic Chemistry

www.elsevier.com/locate/jorganchem

Mechanism of the electrochemical reduction of $[Fe(\eta^5\text{-}C_6H_7)(CO)_3][PF_6]$ — a theoretical approach to the intermediates

M. Fernanda N.N. Carvalho [a,*], M. Amélia N.D.A. Lemos [a], Luís F. Veiros [a], G. Richard Stephenson [b]

[a] *Centro de Química Estrutural, Complexo I, Instituto Superior Técnico, Av. Rovisco Pais, 1049-001 Lisbon, Portugal*
[b] *School of Chemical Sciences, University of East Anglia, Norwich NR4 7TJ, UK*

Received 22 January 2001; accepted 5 March 2001

Abstract

A mechanism is proposed for the electrochemical reduction of $[Fe(\eta^5\text{-}C_6H_7)(CO)_3][PF_6]$ based on cyclic voltammetry and simulation techniques. In $[NBu_4][X]/CH_3CN$ ($X = BF_4$ or ClO_4) but not in $[NBu_4][BF_4]/CH_2Cl_2$, a rapid equilibrium prior to the electron transfer process is identified between $[Fe(\eta^5\text{-}C_6H_7)(CO)_3][PF_6]$ and a species formulated as $[Fe(\eta^3\text{-}C_6H_7)(CO)_3(NCMe)]^+$. The formation of the species under equilibrium involves solvent coordination and η^5 to η^3 ring slippage of the cyclohexadienyl ligand as the response of the system to the high electron count. Electrochemical electron transfer to $[Fe(\eta^3\text{-}C_6H_7)(CO)_3(NCMe)]^+$ affords a highly reactive 19-electron intermediate exhibiting chemical reactivity (ECE mechanism) that leads to the formation of dimer-type species. A 'father–son' type mechanism is proposed for the formation of the products of the electrochemical reduction of $[Fe(\eta^5\text{-}C_6H_7)(CO)_3][PF_6]$. All the species involved in the mechanism were analysed by theoretical means and are proposed on the basis of calculations made with the B3LYP HF/DFT hybrid functional.

Keywords: Mechanism; Cyclohexadienyl; Electrochemistry; Ring slippage; Hapticity change; DFT calculations

1. Introduction

The high reactivity of the cyclohexadienyl ligand coordinated at chromium, iron or manganese in complexes of the type $[M(\eta^5\text{-cyclohexadienyl})(CO)_3]^n$ ($n = 0$ or $+1$) has been successfully used for regio- and stereospecific organic syntheses of alkaloids, steroids and terpenes [1–5]. The processes involve nucleophilic attack at the coordinated six-membered ring directed by its substituents [1,3a] or the entering nucleophile [6]. The involvement of the metal in the process that leads to attack to the π-ligand was proposed in the mechanism of the addition of PMe_3 to the cyclopentadienyl ligand coordinated at $[Ru(\eta^5\text{-}C_5H_5)(\eta^4\text{-}C_5H_4O)L]^+$. In a such case the nucleophilic attack occurs at the metal thus forming a 20-electron intermediate that undergoes η^5 to η^3 ring slippage followed by migration of the phosphine to the ring [7].

Ring slippage from η^5 to η^3 or η^5 to η^1 induced by ligand addition or electrochemical reduction [8–10] at cyclopentadienyl or indenyl ligands has been evidenced by structural analysis, but as far as we know, no such evidence exists in the case of the cyclohexadienyl ligand. The η^3 coordination of cyclohexadienyl was proposed in a few cases [11–13] and it was studied theoretically in a process involving the addition of phosphine to $[Mn(\eta^5\text{-}C_6H_7)(CO)_3]$ [14].

The theoretical results obtained within this work indicate that η^5 to η^3 haptotropic shifts occur at several stages of the process associated to the electrochemical reduction of $[Fe(\eta^5\text{-}C_6H_7)(CO)_3][PF_6]$.

2. Results and discussion

In $[NBu_4][BF_4]/CH_3CN$, $[Fe(\eta^5\text{-}C_6H_7)(CO)_3][PF_6]$ (**1**) displays by cyclic voltammetry (at scan rates between 0.05 and 0.80 V s^{-1}) one irreversible reduction process

* Corresponding author.

0022-328X/01/$ - see front matter
PII: S0022-328X(01)00802-6

at $E_p^{red} = -0.48$ V (wave I) upon which new species are generated that can be detected on the reverse scan [12], Fig. 1(a). Among the new species, the one that oxidises at $E_p^{ox} = 0.96$ V (wave IV) was isolated from bulk-controlled potential electrolysis and identified as [{Fe(CO)$_3$}$_2${μ-(C$_6$H$_7$)$_2$}] (C–C dimer) [12]; the process globally involves transfer of one electron per molecule as measured by coulometry. The minor species ($E_p^{ox} =$ 0.37 V, wave III) conceivably corresponds to [{Fe(η^5-C$_6$H$_7$)(CO)}$_2$(μ-CO)$_2$] (Fe–Fe dimer) [12,13] although it could not be isolated.

In order to get further insight into the mechanism of the electrochemical reduction of [Fe(η^5-C$_6$H$_7$)(CO)$_3$][PF$_6$] we extended the former study made in [NBu$_4$][BF$_4$]/CH$_3$CN to [NBu$_4$][ClO$_4$]/CH$_3$CN or [NBu$_4$][BF$_4$]/CH$_2$Cl$_2$ and higher scan rates (1–30 V s^{-1}).

As observed at lower scan rates, at 1 V s^{-1} in [NBu$_4$][BF$_4$]/CH$_3$CN, waves III and IV form upon reduction at wave I, Fig. 1(a). The intensity of wave III is considerably lower than wave IV, as reported before, for the range of scan rates (0.050–0.80 V s^{-1}) [12]. At scan rates higher than 5 V s^{-1} wave III is not detected, instead at a slightly lower potential ($E_p^{ox} = 0.29$ V) wave (II) is formed with an intensity identical to wave (IV), Fig. 1(b). In the range 2–5 V s^{-1} both waves (II) and (III) are observed.

In acetonitrile, replacing [NBu$_4$][BF$_4$] by [NBu$_4$][ClO$_4$], the redox behaviour of [Fe(η^5-C$_6$H$_7$)(CO)$_3$][PF$_6$] is similar to that reported above, within the range of potentials available.

2.1. Simulation

The experimental data obtained on [Fe(η^5-C$_6$H$_7$)(CO)$_3$][PF$_6$] by cyclic voltammetry in [NBu$_4$]X/CH$_3$CN (X = BF$_4$ or ClO$_4$) or [NBu$_4$][BF$_4$]/CH$_2$Cl$_2$ was analysed by resorting to digital simulation methods (see Section 4).

In [NBu$_4$][BF$_4$]/CH$_3$CN the key experimental observations are: (i) upon dissolution of [Fe(η^5-C$_6$H$_7$)(CO)$_3$][PF$_6$] a reduction process is observed (wave I), Fig. 1(a); (ii) the cathodic wave I broadens with increasing scan rate and its potential shifts to more negative values, in addition to a significant drop in the current function, Fig. 2; (iii) one electron per molecule is transferred at wave I, as measured by coulometry [12]; (iv) there are no original anodic waves but upon reduction, on the reverse scan, new anodic waves are detected, Fig. 1; (v) at scan rates higher than 5 V s^{-1} two waves (waves II and IV) are observed, Fig. 1b; (vi) the intensity of wave II decreases with decreasing scan rate indicating that it corresponds to a short-lived species, at scan rates lower than 2 V s^{-1} wave II is no more visible; (vii) in addition to wave IV, wave III is observed at 1 V s^{-1} and lower scan rates, it could also be detected as a shoulder of wave II, in the range 2–5 V s^{-1}.

In [NBu$_4$][BF$_4$]/CH$_2$Cl$_2$ wave I is a simple one-electron irreversible wave.

2.1.1. Cathodic zone

The data obtained on wave I (see Section 2.1) is characteristic of a CE mechanism (chemical reaction

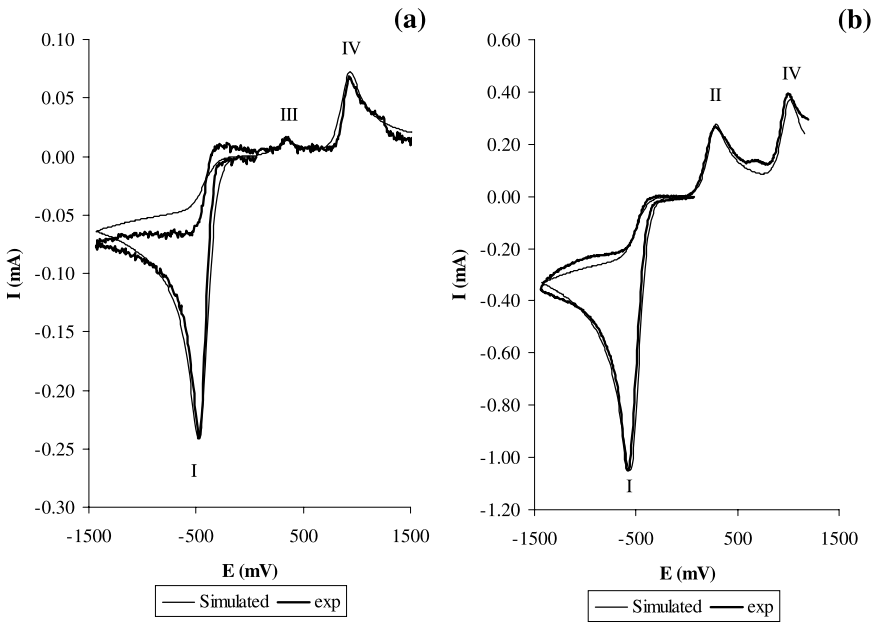

Fig. 1. Experimental and simulated cyclic voltammograms obtained from **1** in [Bu$_4$N][BF$_4$]/CH$_3$CN at: (a) −0.2 V s^{-1} and (b) −5 V s^{-1}.

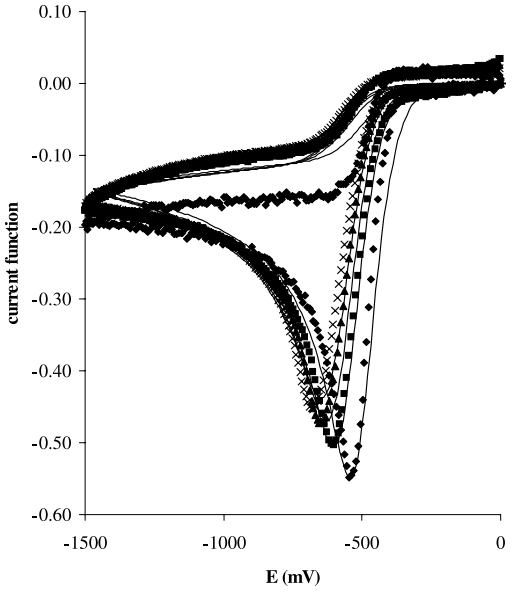

Fig. 2. Current-functions for wave I at different scan-rates: (◆) -0.200 V s^{-1}; (■) -2 V s^{-1}; (△) -5 V s^{-1}; (×) -10 V s^{-1}. The lines correspond to the simulated cyclic voltammograms for the mechanism in Scheme 1 (cathodic).

CATHODIC

$$[Fe(\eta^5\text{-}C_6H_7)(CO)_3]^+ \underset{K_{hom2}}{\overset{K_{hom1}}{\rightleftharpoons}} [Fe(\eta^3\text{-}C_6H_7)(CO)_3(NCMe)]^+$$

$$2[Fe(\eta^3\text{-}C_6H_7)(CO)_3(NCMe)]^+ \xrightarrow{2\,e^-} \begin{cases} \xrightarrow{} A \quad (x\%) \\ \xrightarrow{} C\text{-}C\ dimer \quad (y\%) \end{cases}$$

ANODIC

$$A \xrightarrow[\text{wave II}]{-2\,e^-} Products$$

$$A \xrightarrow{K_{hom3}} Products$$

$$A \xrightarrow{K_{hom4}} Fe\text{-}Fe\ dimer \xrightarrow[\text{wave III}]{-2e^-} Products$$

$$C\text{-}C\ dimer \xrightarrow[\text{wave IV}]{-2\,e^-} Products$$

Scheme 1.

preceding the electron transfer process) [15] involving the equilibrium between two species in solution prior to electron transfer, Scheme 1 (cathodic).

The species in equilibrium with $[Fe(\eta^5\text{-}C_6H_7)(CO)_3][PF_6]$ is assumed to result from the coordination of CH_3CN to the iron centre and η^5 to η^3 slippage of the cyclohexadienyl ring. This type of haptotropic shift was identified structurally on $[Mo(\eta^5\text{-Ind})(CO)_2(NCMe)_2][BF_4]$ (Ind = indenyl) [16a,17] or $[IrCp^*(H)_3(PPh_3)][BF_4]$ ($Cp^* = C_5Me_5$) [16b] upon dissolution in CH_3CN and was reported in some other cases [9]. Despite the similarities of cyclohexadienyl and cyclopentadienyl or indenyl ligands no direct spectroscopic evidence (IR or NMR) has been reported for the coordination of acetonitrile to $[Fe(\eta^5\text{-}C_6H_7)(CO)_3][PF_6]$. Our present study, however, provides some support for the formation of $[Fe(\eta^3\text{-}C_6H_7)(NCMe)(CO)_3][PF_6]$ (**2**) although no experimental evidence could be obtained for any species other than $[Fe(\eta^5\text{-}C_6H_7)(CO)_3][PF_6]$ by IR (in solution) or ^{1}H-NMR (in acetonitrile) within the range -40 to 30°C.

We ascribe the lack of spectroscopic evidence to the fact that the equilibrium between the η^5-complex and the solvent-η^3 (**1** ⇄ **2**) involves fast conversion kinetics, as will be discussed below.

In order to get further evidence for the relevance of CH_3CN to the electrochemical reduction process and support its coordination to the iron centre, we studied the redox behaviour of complex **1** in $[NBu_4][BF_4]/CH_2Cl_2$. Although, the cyclic voltammograms do not differ much of those obtained in acetonitrile, from the simulation it is evident that no equilibrium prior to electron transfer exists, as expected due to the poor coordinating properties of CH_2Cl_2 compared to CH_3CN. Acetonitrile apparently is prone to coordinate transition metal π-ligands coordinating centres. The equilibrium between $[Rh(COD)_2]^+$ and $[Rh(COD)_2(solv)_2]^+$ was also characterised electrochemically [18].

In CH_3CN the values of the equilibrium ($K = 0.5$, $[NBu_4][BF_4]$, or $K = 3.5$, $[NBu_4][ClO_4]$) as well as the kinetic constants (k_{hom1} or k_{hom2}), Table 1, are sensitive to the nature of the electrolyte, although they follow the inverse order, in agreement with the recognised high sensitivity of the system to the reaction conditions.

Tentative simulation of wave I by a process involving the transfer of one electron per molecule, as the total

Table 1
Electrochemical and chemical parameters [a] obtained by simulation of the mechanism in Scheme 1 with different electrolytes

Parameters	Electrolyte	
	$[NBu_4][BF_4]$	$[ClO_4][BF_4]$
E^0 (V)	-0.2	-0.2
k_{hom1} (s^{-1})	800	80
k_{hom2} (s^{-1})	1600	23
k_{het} (cm s^{-1})	1×10^{-4}	1×10^{-4}
α	0.5	0.5

[a] In CH_3CN. Values obtained by fitting of the experimental data within the range 0.050–30 V.

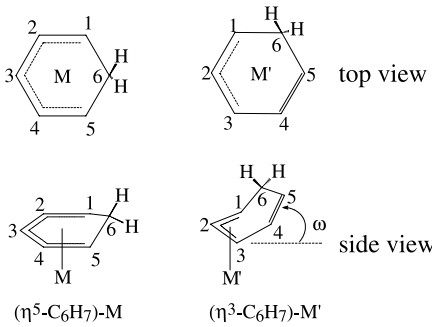

Scheme 2.

number of electrons experimentally measured by controlled potential electrolysis (iii) was unfruitful. The best fits were obtained for the transfer of two electrons with the simultaneous consumption of two iron molecules, but with only one electron being exchanged up to the rate limiting step ($n_\alpha = 1$), Scheme 1 (cathodic). This behaviour is consistent with the transfer of two electrons affording a highly reactive 20-electron species that reacts with the precursor species **1** according to a father–son type mechanism [19]. The transfer of two electrons, in sequence, is corroborated by our theoretical calculations, which indicate that the geometry of the 19-electron intermediate is very close to that of the final species (see below), i.e. η^5 to η^3 ring is induced. A related type of one-electron reduction species was found on the electrochemical reduction of Mo complexes, $[(\eta^5\text{-Ind})CpMoL_2]^{2+}$ (L = CO or $P(OMe)_3$), in which the indenyl ligand in the paramagnetic intermediate $[(\eta^3\text{-Ind})CpMoL_2]^+$, has a folding angle, $\Omega =$ 17°, slightly inferior to the typical values for the η^3 coordination mode (20–30°) [20].

2.1.2. Anodic zone

No anodic waves were detected originally on the cyclic voltammogram of $[Fe(\eta^5\text{-}C_6H_7)(CO)_3][PF_6]$. Upon reduction, the anodic redox behaviour depends strongly on the scan rate. At scan rates equal or lower than 1 V s^{-1}, the main wave IV corresponds to the C–C dimer as previously verified [12]. A low intensity wave (wave III, 0.37 V) is also detected, Fig. 1(a). At scan rates higher than 5 V s^{-1} wave II, attributed to an unidentified short-lived species (**A** in Scheme 1) is observable, Fig. 1(b). At lower scan rates (< 1 V s^{-1}) species **A** is not detected due to fast chemical processes that lead to the formation of an electrochemically silent products (with a kinetic rate constant, k_{hom3}) in addition to a species (Scheme 1, anodic) responsible for wave III that has been tentatively assigned to a Fe–Fe dimer. The exact nature of **A** and that of its products could not be established experimentally, although in complexes with π-ligands dimerisation finds evidence in a few cases [12,13,21].

Using the mechanism proposed in Scheme 1, good fittings to the experimental cyclic voltammograms were obtained. From Figs. 1 and 2 the homogeneous (k_{hom}) and heterogeneous (k_{het}) rate constants (chemical and electrochemical processes, respectively) were evaluated. The parameters for the cathodic processes are displayed in Table 1. The fraction of species **A** ($x = 45\%$) and C–C dimer ($y = 50\%$) were also estimated.

In $[NBu_4][BF_4]$–CH_3CN the fittings also allowed the estimation of the chemical parameters ($k_{hom3} = 0.45$ and $k_{hom4} = 0.10$ s^{-1}), the heterogeneous rate constants ($K_{het2} = K_{het3} = K_{het4} = 1 \times 10^{-4}$ cm s^{-1}) and the transfer coefficients ($\alpha = 0.5$).

2.2. Molecular orbital calculations

In order to test the feasibility of the species that could not be identified experimentally, theoretical calculations by means of DFT [22] and ab initio [23] molecular orbital calculations complemented with the orbital analysis provided by the extended Hückel method [24,25] were performed. An early study on the electronic structure of the cyclohexadienyl ligand and its coordination geometry in $[Fe(\eta^5\text{-}C_6H_7)(CO)_3]^+$ has been done by Hoffmann and Hoffman [26] and later complemented by a study on its reactivity towards nucleophilic addition [27].

The geometrical parameters used to characterise the cyclohexadienyl hapticity through this work are depicted in Scheme 2, being equivalent to those used for other η^5 π-ligands, such as cyclopentadienyl (Cp) or indenyl (Ind) [28]. Since η^5 to η^3 ring slippage corresponds to the elongation of two M–C bond distances (C4 and C5 on Scheme 2) we will use the five Fe–Cx ($x = 1$–5) distances. The angle ω (formed by the planes of the two halves of the folded η^3-$C_6H_7^-$ ligand, i.e. the plane defined by the carbon atoms (C1, C2 and C3) bonded to the metal and the mean plane of C1, C3, C4 and C5) is also used to characterise the geometry. In fact, angle ω thus defined corresponds to the bending angle, Ω, defined by Habib and co-workers [29] to characterise the η^3 coordination on indenyl complexes.

A comparison between ring slippage at cyclohexadienyl and indenyl shows that η^5 to η^3 ring slippage at cyclohexadienyl involves its rotation and introduces an asymmetry at the derived complex due to the formation of a C=C bond between the uncoordinated carbons (C4 and C5, see Scheme 2) not observed in the indenyl complex as already discussed for $[Mn(\eta^3\text{-}C_6H_7)(CO)_3(PH_3)]$ [14].

A geometry optimisation for $[Fe(\eta^5\text{-}C_6H_7)(CO)_3]^+$ was performed in order to test the reliability of the theoretical model used (see Section 4). The optimised structure (Fig. 3) was compared to the crystal structures of the closely related complexes $[Fe(\eta^5\text{-X})(CO)_3]^+$ (X = C_6H_6OMe, $C_6H_5(Me)OMe$ [27] and C_6Me_7 [30])

since from a search on the Cambridge Structural Data Base (CSD) [31] no crystal structure for complex **1** could be found.

The geometrical parameters calculated (see Fig. 3, top) compare well with those reported for the crystal structures specially taking into account that unsubstituted and substituted cyclohexadienyl complexes are considered.

The cyclohexadienyl ligand (Chd) displays a η^5 coordination mode with a negligible bending ($\omega = 2°$) and five similar Fe–C (Chd) bond distances (2.120–2.202 Å) that are in good agreement with the experimental values ($\omega = 2–5°$ and Fe–C (Chd), 2.077–2.269 Å) [26,29].

An important aspect of the η^5-cyclohexadienyl coordination geometry is the out-of-plane bending of methylene group resulting from a repulsive interaction with the metal [26]. In $[Fe(\eta^5\text{-}C_6H_7)(CO)_3]^+$ the value (44°) is comparable to the values for the three iron reference complexes mentioned above (38, 40 and 45° for X = C_6H_6OMe, $C_6H_5(Me)OMe$ and C_6Me_7, respectively)

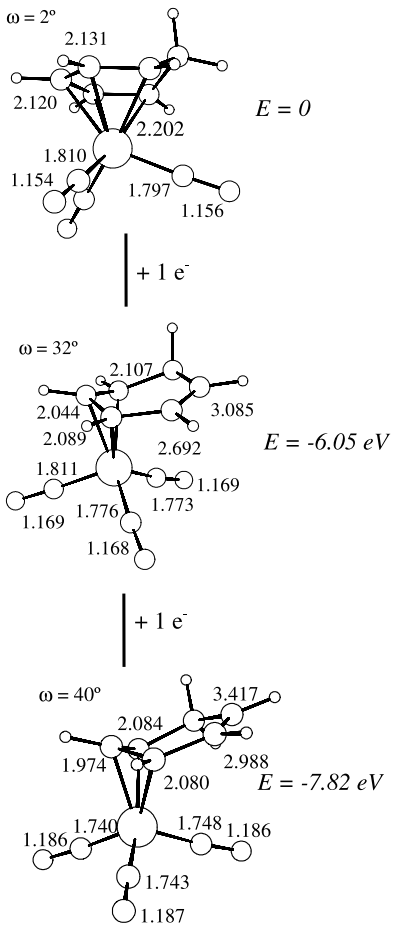

Fig. 3. Optimised structures (B3LYP/3-21G(*)) of the complex $[Fe(\eta^5\text{-}C_6H_7)(CO)_3]^+$ (top) and the species $[Fe(\eta^3\text{-}C_6H_7)(CO)_3]$ (centre) and $[Fe(\eta^3\text{-}C_6H_7)(CO)_3]^-$ (bottom). The more relevant structural parameters (distances in Å) and the relative energies (B3LYP/6-31 + G**) are displayed.

and fits well in the range (40–50°) reported [26] for related complexes derived from other metals.

Moreover, the Fe–C (CO) and C–O bond distances in the calculated (1.797–1.810 and 1.154–1.156 Å, respectively) and experimental structures (1.731–1.899 and 1.122–1.282 Å, respectively) also compare well. In addition, the relative orientation of the cyclohexadienyl towards the carbonyl ligands, with one CO group eclipsing the sp_3 carbon of the cyclohexadienyl ligand (C6 in Scheme 2), is the same in the optimised and the experimental structures. It is worth noticing that although no symmetry constraints were imposed in the optimisation, a C_s structure was obtained.

Since the theoretical method performed well in describing the structure and bonding of $[Fe(\eta^5\text{-}C_6H_7)(CO)_3]^+$ it was used in the evaluation of the species proposed on the mechanism of the electrochemical reduction of **1**.

From the theoretical point of view, the addition of two electrons to an 18-electron complex, either electrochemically or by addition of a ligand, is the simplest way to induce η^5 to η^3 haptotropic shift in a coordinated π-ligand. The excess electron density (20 electrons) on the metal is accommodated by the breaking of two M–C bonds to return to an 18-electron formulation.

2.2.1. $[Fe(\eta^5\text{-}C_6H_7)(CO)_3]^-$

Upon electrochemical reduction of $[Fe(\eta^5\text{-}C_6H_7)(CO)_3]^+$ (through two electrons addition) a 20-electron species forms whose geometry was optimised and the result is shown in Fig. 3 (bottom). The most striking feature of this structure is the clear η^3 coordination mode of the cyclohexadienyl ligand. In fact, this ligand is folded significantly ($\omega = 40°$), in a way that pushes two of the carbon atoms (C4 and C5 in Scheme 2) beyond bonding distances, Fe–C4 = 2.988 and Fe–C5 = 3.417 Å.

In the absence of X-ray data for η^3-coordinated cyclohexadienyl, the calculated parameters are compared with the crystal data of the related complex, $[Fe[(\eta^3\text{-Ind})(CO)_3]^-$ [32], with an η^3 indenyl ligand ($\Omega = 22°$ and two uncoordinated carbon atoms Fe–C = 2.887 and 2.871 Å). The three calculated Fe–C (polyenyl) bond distances (2.084, 1.974 and 2.080 Å for C1–C3, respectively) for the cyclohexadienyl complex and the distances experimentally determined (2.184, 1.995 and 2.193 Å) for the indenyl complex, as well as the distances Fe–C (CO) (1.740–1.748 and 1.741–1.780 Å) and C–O (1.186–1.187 and 1.155–1.173 Å), for the cyclohexadienyl and the indenyl complexes, respectively, compare well, thus providing a high degree of confidence to the optimised structure of $[Fe(\eta^3\text{-}C_6H_7)(CO)_3]^-$.

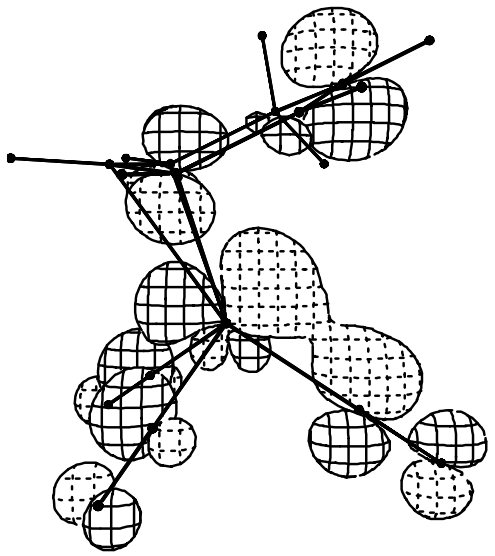

Fig. 4. 3D representation of the HOMO of $[Fe(\eta^3\text{-}C_6H_7)(CO)_3]^-$ generated upon reduction of $[Fe(\eta^5\text{-}C_6H_7)(CO)_3]^+$.

A detailed analysis of the dienyl bonding at $[Fe(\eta^3\text{-}C_6H_7)(CO)_3]^-$ is not necessary due to the similarities with η^3 indenyl and other π-ligands recently published [14,19,27]. Nevertheless, there are some aspects concerning the bonding at the metallic fragment, $\{Fe(CO)_3\}$, that must be addressed. Upon reduction, a shortening of the mean Fe–C (CO) bond distances from 1.81 to 1.74 Å and an augmentation of the C–O mean distances from 1.15 to 1.19 Å is observed as a consequence of an increase in the metal to carbonyl back-donation in the reduced species. This can be traced to the $[Fe(\eta^3\text{-}C_6H_7)(CO)_3]^-$ highest occupied molecular orbital (HOMO) (Fig. 4). Furthermore, this is the orbital which becomes occupied upon electrochemical reduction and it presents a Fe–(Chd) π^* character, as shown in Fig. 4. The stabilisation of this orbital, i.e. freed from its anti-bonding character, is the driving force to the η^5 to η^3 haptotropic shift that is accomplished by the elongation of two Fe–C distances, as previously mentioned for indenyl [20] and other π-ligands [14,27] involved in ring slippage.

2.2.2. $[Fe(\eta\text{-}C_6H_7)(CO)_3]$

In the proposed mechanism for the electrochemical reduction of **1**, Scheme 1, two electrons per molecule are involved in a process that under the electrochemical point of view occurs through $1 + 1$ electron transfer. In order to test this possibility a spin unrestricted calculation was performed to optimise the structure of the paramagnetic species $[Fe(\eta\text{-}C_6H_7)(CO)_3]$ that would form upon one-electron transfer to **1**. The more relevant structural parameters and the relative energies calculated for $[Fe(\eta\text{-}C_6H_7)(CO)_3]$ are depicted in Fig. 3 (centre). The structure displays intermediate values between $[Fe(\eta^5\text{-}C_6H_7)(CO)_3]^+$ and those of the fully reduced species, $[Fe(\eta^3\text{-}C_6H_7)(CO)_3]^-$ (Fe–C (CO) and C–O mean distances are 1.79 and 1.17 Å, respectively), while the Fe–C (Chd) bonding distances (2.044–2.107 Å) are in the range of those discussed above.

A relevant aspect evidenced by the optimised structure is a clear η^3 cyclohexadienyl coordination in the one-electron reduced species $[Fe(\eta\text{-}C_6H_7)(CO)_3]$, as shown by the bending angle ($\omega = 32°$) and the two long Fe–C4/5 distances (2.692 and 3.085 Å). Hence, the optimised structure is closer to the fully reduced species than to **1** as shown by the geometrical parameters. Such a process has been verified on the reduction of the indenyl complex $[Mo(\eta^5\text{-Ind})(Cp)(CO)_2]^{2+}$ [20].

The theoretical results are in excellent agreement with the mechanism proposed for the electrochemical reduction of $[Fe(\eta^5\text{-}C_6H_7)(CO)_3]^+$ which assumed $1 + 1$ electrons are transferred, the first electron transfer being the rate limiting step at the reduction process.

2.2.3. $[Fe(\eta^3\text{-}C_6H_7)(CO)_3(NCMe)]^+$

In the mechanism proposed for the electrochemical reduction of $[Fe(\eta^5\text{-}C_6H_7)(CO)_3]^+$ there is a kinetic evidence for the formation of a species formulated as $[Fe(\eta^3\text{-}C_6H_7)(CO)_3(NCMe)]^+$ (**2**) that could not be confirmed experimentally. Such a process involving addition of the solvent (CH_3CN) and ring slippage was determined undoubtedly by structural analysis upon dissolution of $[Mo(\eta^5\text{-Ind})(CO)_2(NCMe)_2]^{2+}$ in CH_3CN [17].

To verify the ability of the Fe–cyclohexadienyl system to undergo such a process and support our proposal, a theoretical investigation was made with HCN used as a model for CH_3CN since no major disadvantages result [17].

From the theoretical calculations it emerges that $[Fe(\eta^3\text{-}C_6H_7)(CO)_3(HCN)]^+$ (**2′**) (Fig. 5, bottom) has a distorted octahedral structure with the cyclohexadienyl ligand occupying two adjacent positions, as expected for a d^6 complex. The overall geometry is analogous to that calculated for $[Mn(\eta^3\text{-}C_6H_7)(CO)_3(PH_3)]$ [14] and to that determined by X-ray for $[Mn(\eta^3\text{-}C_{10}H_9)(CO)_3\{P(OMe)_3\}]$ [33]. In the latter complex the π-ligand (1-hydronaphthalene) formally corresponds to a cyclohexadienyl with a fused benzene ring.

From the calculations it is evident that the incoming nitrile coordinates (Fe–N = 1.952 Å) in a position that simultaneously minimises the steric repulsion with cyclohexadienyl and avoids two carbonyls *trans* to each other [14].

A clear η^3-cyclohexadienyl coordination is found at $[Fe(\eta^3\text{-}C_6H_7)(CO)_3(HCN)]^+$ as shown by the significant folding angle ($\omega = 33°$) and the two long Fe–C (Chd) distances (3.216 and 3.499 Å).

The carbonyl bond distances (Fe–C(CO) (1.773–1.829 Å) and C–O (1.156–1.158 Å)] indicate a back-donation similar to that found for the $[Fe(\eta^3\text{-}C_6H_7)(CO)_3]^-$ (see above).

The transition state for the addition of nitrile to $[(\eta^5\text{-}C_6H_7)Fe(CO)_3]^+$ was also identified and its geometry optimised (see Section 4), Fig. 5, top. The calculated structure is close to that of the final species $[(\eta^3\text{-}C_6H_7)Fe(CO)_3(HCN)]^+$ (Fig. 5, bottom), i.e. the cyclohexadienyl ligand displays a coordination geometry with a significant folding angle ($\omega = 29°$) and bond distances are similar to the η^3 complexes values, e.g. Fe–C1/2/3 (2.083–2.200), Fe–C4/5 (2.772–3.118), Fe–C (CO) (1.759–1.809) and C–O (1.156–1.158).

The Chd coordination geometry and the relatively shorter Fe–N distance (2.761 Å) suggest that the cyclohexadienyl η^5 to η^3 ring slippage is the factor that controls the solvent addition, since most of the geometrical distortion occurs before the transition state as previously reported for the addition of PH_3 to $[Mn(\eta^5\text{-}Chd)(CO)_3]$ [14].

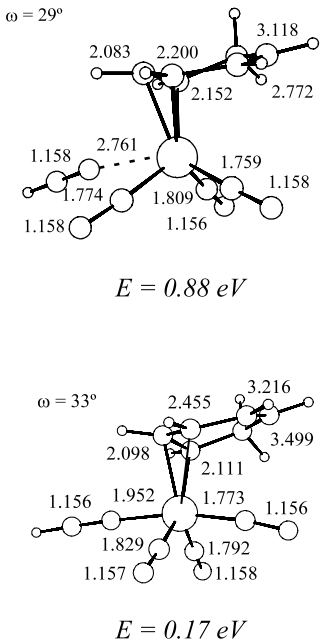

Fig. 5. Optimised structures (B3LYP/3-21G(*)) for the complex $[Fe(\eta^5\text{-}C_6H_7)(CO)_3(HCN)]^+$ (bottom) and the transition state for the HCN addition (top). The more relevant structural parameters (distances in Å) and the energies (B3LYP/6-31 + G**) relative to the reactants ($[(\eta^5\text{-}C_6H_7)Fe(CO)_3]^+ + HCN$) are also represented.

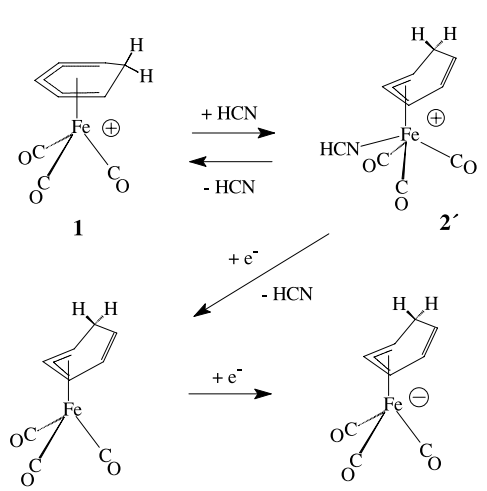

Scheme 3.

The small energy barrier ($\Delta E_a = 0.88$ eV) to form $[Fe(\eta^5\text{-}C_6H_7)(CO)_3(NCMe)]^+$ suggests a spontaneous process at room temperature thus reinforcing the proposal that, in acetonitrile, $[Fe(\eta^3\text{-}C_6H_7)(CO)_3(NCMe)]^+$ is the species in equilibrium with $[Fe(\eta^5\text{-}C_6H_7)(CO)_3]^+$.

Further calculations to establish the fate of **2** upon one-electron reduction revealed that elimination of the solvent is favourable (by 0.48 eV) compared to the possible formation of $[Fe(\eta^3\text{-}C_6H_7)(CO)_3(HCN)]$, Scheme 3.

3. Conclusions

In acetonitrile $[Fe(\eta^5\text{-}C_6H_7)(CO)_3]^+$ establishes an equilibrium, prior to electron transfer, with $[Fe(\eta^3\text{-}C_6H_7)(CO)_3(NCMe)]^+$ due to fast reversible addition of the solvent. Furthermore, the η^5 to η^3 hapticity change of the cyclohexadienyl ligand occurs. The DFT theoretical calculations confirm that the species in equilibrium are energetically similar and support their ability for fast interconversion. This is the first evidence for cyclohexadienyl ring slippage and acetonitrile coordination to form $[Fe(\eta^3\text{-}C_6H_7)(NCMe)(CO)_3]^+$.

The electrochemical reduction does not involve direct electron transfer to $[Fe(\eta^5\text{-}C_6H_7)(CO)_3]^+$. The mechanism occurs through 1 + 1 electron transfer to $[Fe(\eta^3\text{-}C_6H_7)(NCMe)(CO)_3]^+$ with the total of one electron being consumed in the process, in agreement with a 'father–son' type mechanism.

The detailed theoretical study of the intermediates involved in the process reveals that η^5 to η^3 ring slippage occurs upon transfer of the first electron with solvent loss and formation of $[Fe(\eta^3\text{-}C_6H_7)(CO)_3]$. Upon the transfer of the second electron the highly reactive species $[Fe(\eta^5\text{-}C_6H_7)(CO)_3]^-$ forms and undergoes fast reaction through two possible routes (see Scheme 1) to afford the final C–C or Fe–Fe dimers.

Since acetonitrile is used commonly as the solvent for organic reactions of $[Fe(\eta^5\text{-}C_6H_7)(CO)_3]^+$ salts with nucleophiles, the electrochemical and DFT data presented have indicated that reversible addition of acetonitrile needs to be taken into account when considering rearrangement in these systems.

4. Experimental

The complex $[Fe(\eta^5\text{-}C_6H_7)(CO)_3][PF_6]$ was prepared as reported [34]. The electrochemical studies were done in a Radiometer DEA 101 Digital electrochemical

analyser interfaced with an IMT 102 Electrochemical Interface, using a 0.2 M $[NBu_4][BF_4]/CH_3CN$, $[BF_4][ClO_4]/CH_3CN$ or $[NBu_4][BF_4]/CH_2Cl_2$ solution. The solvents were pre-dried over CaH_2 and distilled immediately before use. All the experiments were carried out under inert atmosphere. Pt wire was used as a working electrode for cyclic voltammetry.

4.1. Digital simulation

Digital simulations were performed with software developed in Turbo Pascal Version 6 (Borland International©). The relevant partial differential equations were solved by the 'method of lines', using an exponentially expanding space grid, according to the following expression:

$$\Delta x_i = \Delta x_0 \, e^{\beta i} \quad i = 0,1,\ldots,n$$

This approach was proposed initially by Pletcher and Joslin [35] for the finite difference method and has been extended to the 'method of lines' in a previous work [36]. The expansion parameter (β) used in these simulations was 0.1, and the width of the first element (Δx_i) was computed so that the total diffusion layer met the estimation, made for each individual voltammogram, according to Ref. [37].

The integration of the ordinary differential equations obtained after space discretisation was performed by the fourth-order Runge–Kutta method, which was shown to be suitable for these problems, with respect to stability, computation time and error level, as discussed previously [38]. The experimental cyclic voltammograms were baseline corrected for comparison with the theoretical ones.

The program was run on a Pentium II 450 MHz personal computer.

4.2. Molecular orbital calculations

The geometry optimisations were accomplished by means of ab initio and DFT calculations performed with the GAUSSIAN-98 program [39]. The B3LYP hybrid functional with a 3-21G(*) basis set [40] was used in all optimisations. This functional includes a mixture of Hartree–Fock [23] exchange with DFT [22] exchange-correlation, given by Becke's three-parameter functional [41] with the Lee, Yang and Parr correlation functional, which includes both local and non-local terms [42,43]. All the optimised geometries are the result of full optimisations without any symmetry constraints. Single point calculations were run on the optimised structures at the same theory level with a 6-31 + G** basis set [44].

The transition state optimisation was performed, at the same level of theory, with the synchronous transit-guided quasi-Newton method (STQN) developed by Schlegel and co-workers [45]. The transition state determination was confirmed by a frequency calculation yielding one imaginary frequency, and also by small displacements along the reaction path in both directions, resulting in the reactants and the products, respectively.

The extended Hückel calculations [23,24] were done with the CACAO program [46] and modified H_{ij} values were used [47]. The basis set for the metal atom consisted of ns, np and $(n-1)$d orbitals. The s and p orbitals were described by single Slater-type wavefunctions, and the d orbitals were taken as contracted linear combinations of two Slater-type wavefunctions. The parameters used for Fe were the following (H_{ii} (eV), ζ): 4s −9.170, 1.900; 4p −5.370, 1.900; 3d −12.700, 5.350, 1.800 (ζ_2), 0.5366 (C_1), 0.6678 (C_2). Standard parameters were used for other atoms. Calculations were performed on models based on the optimised geometries with idealised maximum symmetry, and following are the distances (Å): Fe–C (cyclohexadienyl) 2.20, Fe–C (CO) 1.82, Fe–N 1.90, C–O 1.15, C–C 1.40, C–N 1.13, C–H 1.08; and angles (°): (C_6H_7)–Mn–CO 120.0 ($[(\eta\text{-}C_6H_7)Fe(CO)_3]^{+/0/-}$ complexes).

Acknowledgements

The authors gratefully acknowledge Dr M.F. Minas da Piedade for help with the CSD. The Fundação para a Ciência e Tecnologia (FCT) and Praxis XXI Program are acknowledged for financial support.

References

[1] A. Pearson (Ed.), Metallo-Organic Chemistry, Wiley, Chichester, 1988 (Ch. 8).
[2] (a) F. Urbanos, M.A. Halcrow, J. Fernandez-Baeza, F. Dahan, D. Labroue, B. Chaudret, J. Am. Chem. Soc. 115 (1993) 3484; (b) M.A. Halcrow, F. Urbanos, B. Chaudret, Organometallics 12 (1993) 955.
[3] (a) G.R. Stephenson, S.T. Astley, I.M. Palotai, in: K.H. Dötz, R.W. Hoffmann (Eds.), Regiocontrolled Applications of Transition Metal π-complexes in Organic Synthesis via Organometallics, Vieweg, Braunschweig, 1991, pp. 169–185;
(b) S.T. Astley, M. Mayer, G.R. Stephenson, Tetrahedron Lett. 34 (1993) 2035.
[4] (a) K. Woo, P.G. Williard, D.A. Sweigart, N.W. Duffy, B.H. Robinson, J. Simpson, J. Organomet. Chem. 487 (1995) 111;
(b) K. Woo, G.B. Carpenter, D.A. Sweigart, Inorg. Chim. Acta 220 (1994) 297.
[5] A. Fretzen, A. Ripa, R. Liu, G. Bernardinelli, E.P. Kündig, Chem. Eur. J. 2 (1998) 251.
[6] I. Verona, J.P. Gutheil, R.D. Pike, G.B. Carpenter, J. Organomet. Chem. 524 (1996) 71.
[7] W. Simanko, V.S. Sapunov, R. Schmid, K. Kirchner, Organometallics 17 (1998) 2391.
[8] D. Astruc, Electron Transfer and Radical Processes in Transition-Metal Chemistry, VCH, New York, 1995.
[9] J.M. O'Connor, C.P. Casey, Chem. Rev. 87 (1987) 307.

[10] K.A. Pevear, H. Banaszak, G.B. Carpenter, A.L. Rieger, P.H. Rieger, D.A. Sweigart, Organometallics 14 (1995) 512.
[11] C. Zou, K.J. Ahmed, M.S. Wrighton, J. Am. Chem. Soc. 111 (1989) 1133.
[12] M.F.N.N. Carvalho, A.J.L. Pombeiro, I.M. Shrophire, G.R. Stephenson, Inorg. Chim. Acta 248 (1996) 45.
[13] R.E. Lehmann, J.K. Kochi, Organometallics 10 (1991) 190.
[14] L.F. Veiros, Organometallics 19 (2000) 3127.
[15] A.J. Bard, L.R. Faulker, Electrochemical Methods. Fundamentals and Applications, Wiley, New York, 1980.
[16] (a) J.R. Ascenso, I.S. Gonçalves, E. Herdtweck, C.C. Romão, J. Organomet. Chem. 508 (1996) 169;
(b) A. Pedersen, M. Tilset, Organometallics 12 (1993) 3064.
[17] M.J. Calhorda, C.A. Gamelas, I.S. Gonçalves, E. Herdtweck, C.C. Romão, L.F. Veiros, Organometallics 17 (1998) 2597.
[18] J. Orsini, W.E. Geiger, Organometallics 18 (1999) 1854.
[19] C. Amatore, A. Ceccon, S. Santi, J.-N. Verpeaux, Chem. Eur. J. 3 (1997) 279.
[20] M.J. Calhorda, L.F. Veiros, Coord. Chem. Rev. 185–186 (1999) 37.
[21] R.F. Winter, W.E. Geiger, Organometallics 18 (1999) 1827.
[22] R.G. Parr, W. Yang, Density Functional Theory of Atoms and Molecules, Oxford University Press, New York, 1989.
[23] W.J. Hehre, L. Radom, P.v.R. Schleyer, J.A. Pople, Ab Initio Molecular Orbital Theory, Wiley, New York, 1986.
[24] R. Hoffmann, J. Chem. Phys. 39 (1963) 1397.
[25] R. Hoffmann, W.N. Lipscomb, J. Chem. Phys. 36 (1962) 2179.
[26] R. Hoffmann, P. Hoffman, J. Am. Chem. Soc. 98 (1976) 598.
[27] O. Eisenstein, W.M. Butler, A.J. Pearson, Organometallics 3 (1984) 1150.
[28] L.F. Veiros, J. Organomet. Chem. 587 (1999) 221.
[29] J.W. Faller, R.H. Crabtree, A. Habib, Organometallics 4 (1985) 929.
[30] Yu.V. Gatilov, N.G. Bokii, Yu.T. Struchkov, Zh. Strukt. Khim. 16 (1975) 855 (references taken from the CSD).
[31] F.H. Allen, J.E. Davies, J.J. Galloy, O. Johnson, O. Kennard, C.F. Macrae, D.G. Watson, J. Chem. Inf. Comput. Sci. 31 (1991) 204.
[32] T.C. Forschner, A.R. Cutler, R.K. Kullnig, Organometallics 6 (1987) 889.
[33] S.U. Son, S.-J. Paik, I.S. Lee, Y.-A. Lee, Y.K. Chung, W.K. Seok, H.N. Lee, Organometallics 18 (1999) 4114.
[34] E.O. Fischer, R.D. Fischer, Angew. Chem. 72 (1960) 919.
[35] J. Joslin, D. Pletcher, J. Electroanal. Chem. 49 (1974) 171.
[36] M.A.N.D.A. Lemos, A.J.L. Pombeiro, Port. Electrochim. Acta 10 (1992) 89.
[37] D. Britz, Digital Simulation in Electrochemistry, 2nd ed., Springer, Berlin, 1988.
[38] M.A.N.D.A. Lemos, A.J.L. Pombeiro, in: A.J.L. Pombeiro, J. McCleverty (Eds.), Molecular Electrochemistry of Inorganic, Bioinorganic and Organometallic Compounds. In: NATO ASI Series C, vol. 385, Kluwer, Dordrecht, 1993, p. 477.
[39] M.J. Frisch, G.W. Trucks, H.B. Schlegel, G.E. Scuseria, M.A. Robb, J.R. Cheeseman, V.G. Zakrzewski, J.A. Montgomery, Jr., R.E. Stratmann, J.C. Burant, S. Dapprich, J.M. Millam, A.D. Daniels, K.N. Kudin, M.C. Strain, O. Farkas, J. Tomasi, V. Barone, M. Cossi, R. Cammi, B. Mennucci, C. Pomelli, C. Adamo, S. Clifford, J. Ochterski, G.A. Petersson, P.Y. Ayala, Q. Cui, K. Morokuma, D.K. Malick, A.D. Rabuck, K. Raghavachari, J.B. Foresman, J. Cioslowski, J.V. Ortiz, B.B. Stefanov, G. Liu, A. Liashenko, P. Piskorz, I. Komaromi, R. Gomperts, R.L. Martin, D.J. Fox, T. Keith, M.A. Al-Laham, C.Y. Peng, A. Nanayakkara, C. Gonzalez, M. Challacombe, P.M.W. Gill, B. Johnson, W. Chen, M.W. Wong, J.L. Andres, C. Gonzalez, M. Head-Gordon, E.S. Replogle, J.A. Pople, GAUSSIAN-98, Revision A.6, Gaussian Inc., Pittsburgh, PA, 1988.
[40] (a) J.S. Binkley, J.A. Pople, W.J. Hehre, J. Am. Chem. Soc. 102 (1980) 939;
(b) M.S. Gordon, J.S. Binkley, J.A. Pople, W.J. Pietro, W.J. Hehre, J. Am. Chem. Soc. 104 (1982) 2797;
(c) W.J. Pietro, M.M. Francl, W.J. Hehre, D.J. Defrees, J.A. Pople, J.S. Binkley, J. Am. Chem. Soc. 104 (1982) 5039;
(d) K.D. Dobbs, W.J. Hehre, J. Comput. Chem. 7 (1986) 359;
(e) K.D. Dobbs, W.J. Hehre, J. Comput. Chem. 8 (1987) 861;
(f) K.D. Dobbs, W.J. Hehre, J. Comput. Chem. 8 (1987) 880.
[41] A.D. Becke, J. Chem. Phys. 98 (1993) 5648.
[42] C. Lee, W. Yang, R.G. Parr, Phys. Rev. B 37 (1988) 785.
[43] B. Miehlich, A. Savin, H. Stoll, H. Preuss, Chem. Phys. Lett. 157 (1989) 200.
[44] (a) R. Ditchfield, W.J. Hehre, J.A. Pople, J. Chem. Phys. 54 (1971) 724;
(b) W.J. Hehre, R. Ditchfield, J.A. Pople, J. Chem. Phys. 56 (1972) 2257;
(c) P.C. Hariharan, J.A. Pople, Mol. Phys. 27 (1974) 209;
(d) M.S. Gordon, Chem. Phys. Lett. 76 (1980) 163;
(e) P.C. Hariharan, J.A. Pople, Theor. Chim. Acta 28 (1973) 213.
[45] (a) C. Peng, P.Y. Ayala, H.B. Schlegel, M.J. Frisch, J. Comput. Chem. 17 (1996) 49;
(b) C. Peng, H.B. Schlegel, Isr. J. Chem. 33 (1994) 449.
[46] C. Mealli, D.M. Proserpio, J. Chem. Ed. 67 (1990) 39.
[47] J.H. Ammeter, H.-J. Bürgi, J.C. Thibeault, R. Hoffmann, J. Am. Chem. Soc. 100 (1978) 3686.